Conditions for Stability of Droop–Controlled Inverter–Based Microgrids

Johannes Schiffer[a,*], Romeo Ortega[b], Alessandro Astolfi[c], Jörg Raisch[d], Tevfik Sezi[e]

[a] *Technische Universität Berlin, Einsteinufer 11, 10587 Berlin, Germany*
[b] *Laboratoire des Signaux et Systémes, École Supérieure d'Electricité (SUPELEC), Gif-sur-Yvette 91192, France*
[c] *Department of Electrical and Electronic Engineering, Imperial College London, London SW7 2AZ, U.K., & Dipartimento di Informatica, Sistemi e Produzione (DISP), University of Rome Tor Vergata, 00133 Rome, Italy*
[d] *Technische Universität Berlin & Max-Planck-Institut für Dynamik komplexer technischer Systeme, Sandtorstr. 1, 39106 Magdeburg, Germany*
[e] *Siemens AG, Smart Grid Division, Energy Automation, Humboldtstr. 59, 90459 Nuremberg, Germany*

Abstract

We consider the problem of stability analysis of droop-controlled inverter–based microgrids with meshed topologies. The inverter models include variable frequencies as well as voltage amplitudes. Conditions on the tuning gains and setpoints for frequency and voltage stability, together with desired power sharing, are derived in the paper. First, we prove that for all practical choices of these parameters global boundedness of trajectories is ensured. Subsequently, assuming the microgrid is lossless, a port–Hamiltonian description is derived from which sufficient conditions for local asymptotic stability are given. Finally, we propose a design criterion on the controller gains such that a desired active power distribution is achieved in steady-state. Our analysis is further validated via a simulation example of a microgrid based on the CIGRE benchmark medium voltage distribution network.

Keywords: microgrid control, microgrid stability, smart grid applications, inverters, droop control, port-Hamiltonian systems, power sharing

1. Introduction

Motivated by environmental, economic and technological aspects, the penetration of renewable energy sources into the electrical networks is increasing worldwide. Most of these sources are small-scale distributed generation (DG) units connected at the low voltage (LV) and medium voltage (MV) levels via alternating current (AC) inverters. As a consequence, the power generation structure is moving from purely large, centralized plants to a mixed generation pool consisting of conventional large plants and smaller distributed generation units. Since in addition, the physical characteristics of inverters largely differ from the characteristics of conventional electrical generators (*i.e.* synchronous generators (SGs)), new concepts and strategies to operate the electric power system that ensure a reliable and stable operation are needed.

The microgrid concept represents one promising solution to address these issues by facilitating local integration of renewable energy sources [19, 14]. In general, a microgrid gathers a combination of generation units, loads and energy storage elements at distribution level into a locally controllable system, which can be operated in a decentralized and completely isolated manner from the main transmission system. An autonomous or islanded microgrid is operated in the latter mode. The microgrid concept has been identified as a key component in future electrical networks [9]. Furthermore, it is envisioned to greatly contribute to the implementation of numerous smart grid functions [20].

In this work, we consider the problem of frequency and voltage stability in a microgrid while sharing the power demand among the different generation units. The problem of power sharing mainly addresses the following question: how should the different generation units in the network adjust their output power upon load changes in the system to fulfill the demand while satisfying a desired power distribution? It is required that these objectives are achieved in a decentralized way without communication among units, thereby allowing a plug–and–play–like operation [19].

A control technique widely used to address this problem for active power in large power systems is droop control, also referred to as power–speed characteristic [17]. In droop control the current value of the rotational speed of each SG in the network is monitored locally to derive how

*Corresponding author J. Schiffer. Tel. +49-30-314-23573. Fax +49-30-314-21137.

Email addresses: schiffer@control.tu-berlin.de (Johannes Schiffer), ortega@lss.supelec.fr (Romeo Ortega), a.astolfi@ic.ac.uk (Alessandro Astolfi), raisch@control.tu-berlin.de (Jörg Raisch), tevfik.sezi@siemens.com (Tevfik Sezi)

much mechanical power each SG needs to provide. From a control perspective, droop control is a proportional controller where the control gain (known as droop gain) specifies the steady–state power distribution in the network. Since performance under droop control is satisfactory for large systems, this technique has been adapted to inverters [3, 4, 33, 1].

Further, in large transmission systems droop-control is usually only applied to obtain a desired active power distribution, while the voltage amplitude at a generator bus is regulated to a nominal voltage setpoint via an automatic voltage regulator (AVR) acting on the excitation system of the SG. In microgrids the power lines are typically relatively short. Then, the AVR employed at the transmission level is in general not appropiate since slight differences in voltage amplitudes can cause high reactive power flows. As a consequence the reactive power sharing among generation units cannot be ensured. Therefore, droop control is typically also applied to achieve a desired reactive power distribution in inverter-based networks. The most common approach is to control the voltage amplitude with a proportional control, the feedback signal of which is the reactive power generation relative to a reference setpoint [3, 4], see also the recent survey [11].

The paper is devoted to the stability analysis of droop–controlled microgrids. As in any conventional power system, stability is understood in the sense of achieving asymptotic synchronization of the frequencies of all DG units, with the angle differences not exceeding $\frac{\pi}{2}$ and constant generated voltages [18]. Since the synchronization frequency is the same for all DG units and their dynamics depends on the angle differences, it is possible to translate—via a time–dependent coordinate shift—the synchronization objective into a standard (constant) equilibrium stabilization problem, which is the approach adopted in the paper.

Most early stability analysis of droop-controlled microgrids has been carried out by means of detailed numerical small-signal analysis as well as extensive simulations and experimental studies aiming to characterize a range for the droop gains guaranteeing system stability [4, 33, 26, 1]. However, as pointed out in [11], most work on microgrid stability has so far focussed on radial microgrids. Furthermore, it is concluded in [11], that stability of microgrids with meshed topologies and decentralized controlled units is still an open research area.

For radial lossless microgrids, and under the assumption of constant voltage amplitudes, analytic conditions for proportional power sharing and synchronization of lossless microgrids with first-order inverter models have been derived in [31] applying results of the theory of coupled oscillators. Conditions for voltage stability for a lossless parallel microgrid with one common load have been derived in [32].

For general meshed networks, with the aim to schedule the droop coefficients under the consideration of frequency droop, an iterative procedure based on bifurcation theory has been proposed in [6]. Under the assumption of constant voltage amplitudes, analytic synchronization conditions for a lossy meshed microgrid with distributed rotational and electronic generation are derived in [30] using ideas from second order consensus algorithms. A decentralized LMI-based control design for lossy meshed inverter-based networks guaranteeing overall network stability for the nonlinear model considering variable voltage amplitudes and phase angles while accounting for power sharing is provided in [29].

The main contribution of the paper is to give conditions on the droop gains to ensure stability of droop-controlled inverter-based microgrid with general meshed topology and inverter models with variable frequencies as well as variable voltage amplitudes. In contrast to [31, 32, 30], no assumptions of constant voltage amplitudes or small phase angle differences are made. In this more general scenario, the graph theoretic methods employed in the aforementioned papers are not directly applicable. Instead, we adopt a classical Lyapunov–like approach for analysis of stability of equilibria and boundedness of trajectories. Conditions for global boundedness are given for lossy microgrids. Following the interconnection and damping assignment passivity–based control approach [24], we represent the lossless microgrid system in port–Hamiltonian form [28] to identify the energy–Lyapunov function and give conditions for asymptotic stability of the frequency synchronization equilibrium state.

The remaining of the paper is organized as follows. The network model is presented in Section 2. In Section 3 we give the model of the inverter and the droop control. Section 4 presents conditions for global boundedness of trajectories. Sufficient conditions for local asymptotic stability are established in Section 5. In Section 6 we propose a selection of the droop gains, similar to the one given in [31], that ensures the DG units share (in steady-state) the active power according to a specified pattern. Our analysis is validated in Section 7 with a simulation example based on the CIGRE (Conseil International des Grands Réseaux Electriques) benchmark MV distribution network [27]. The paper is wrapped–up with some conclusions and future work in Section 8.

Notation We define the sets $\bar{n} := \{1, \dots, n\}$, $\mathbb{R}_{\geq 0} := \{x \in \mathbb{R} | x \geq 0\}$, $\mathbb{R}_{>0} := \{x \in \mathbb{R} | x > 0\}$ and $\mathbb{S} := [0, 2\pi]$. For a set $\mathcal{U} := \{\nu_1, \dots, \nu_n\}$, $i \sim \mathcal{U}$ denotes $i = \nu_1, \dots, \nu_n$. Let $x := \mathrm{col}(x_i) \in \mathbb{R}^n$ denote a vector with entries x_i for $i \sim \bar{n}$, $\underline{0}_n \in \mathbb{R}^n$ the vector of all zeros, $\mathbb{1}_n \in \mathbb{R}^n$ the vector with all ones, and $\mathrm{diag}(a_i), i = 1, \dots n$ an $n \times n$ diagonal matrix with entries a_i. The notation $\mathrm{blkdiag}(B_1, B_2)$ denotes a block diagonal matrix with diagonal entries B_1, B_2. Let j denote the imaginary unit. Also, ∇f denotes the transpose of the gradient of a function $f : \mathbb{R}^n \to \mathbb{R}$.

2. Network model

We consider a generic meshed microgrid and, following the classical approach in conventional power system studies, assume that loads are modeled by constant impedances [34]. This leads to a set of nonlinear differential–algebraic equations (DAE). Then, a network reduction (called Kron reduction [17]) is carried out to eliminate all algebraic equations corresponding to loads and obtain a set of differential equations. We assume this process has been carried out and work with the Kron–reduced network.

The Kron–reduced microgrid is formed by n nodes, each of which represents a DG unit interfaced via an AC inverter. We associate a time-dependent phase angle $\delta_i : \mathbb{R}_{\geq 0} \to \mathbb{S}$ and a voltage amplitude $V_i : \mathbb{R}_{\geq 0} \to \mathbb{R}_{>0}$ to each node $i \in \bar{n}$ in the microgrid. Then, two nodes i and k of the microgrid are connected via a complex admittance $Y_{ik} := G_{ik} + jB_{ik} \in \mathbb{C}$ with conductance $G_{ik} \in \mathbb{R}$ and susceptance $B_{ik} \in \mathbb{R}$. We denote the set of network nodes by $\bar{n}$ and the set of neighbors of a node $i \in \bar{n}$ by $\mathcal{N}_i := \{k \mid k \in \bar{n},\ k \neq i\ , Y_{ik} \neq 0\}$. For ease of notation, we write angle differences as $\delta_{ik} := \delta_i - \delta_k$.

The active and reactive power flows $P_{ik} : \mathbb{S}^2 \times \mathbb{R}^2_{>0} \to \mathbb{R}$, $Q_{ik} : \mathbb{S}^2 \times \mathbb{R}^2_{>0} \to \mathbb{R}$ from node $i \in \bar{n}$ to node $k \in \bar{n}$ are then given by [17]

$$\begin{aligned} P_{ik}(t) =& G_{ik}V_i^2(t) \\ &- V_i(t)V_k(t)(G_{ik}\cos(\delta_{ik}(t)) + B_{ik}\sin(\delta_{ik}(t))) \\ Q_{ik}(t) =& -B_{ik}V_i^2(t) \\ &- V_i(t)V_k(t)(G_{ik}\sin(\delta_{ik}(t)) - B_{ik}\cos(\delta_{ik}(t))). \end{aligned} \tag{1}$$

The overall active and reactive power flows $P_i : \mathbb{S}^n \times \mathbb{R}^n_{>0} \to \mathbb{R}$, $Q_i : \mathbb{S}^n \times \mathbb{R}^n_{>0} \to \mathbb{R}$ at a node $i \in \bar{n}$ are obtained as[1]

$$\begin{aligned} P_i =& G_{ii}V_i^2 - \sum_{k\sim\mathcal{N}_i} V_iV_k(G_{ik}\cos(\delta_{ik}) + B_{ik}\sin(\delta_{ik})) \\ Q_i =& -B_{ii}V_i^2 - \sum_{k\sim\mathcal{N}_i} V_iV_k(G_{ik}\sin(\delta_{ik}) - B_{ik}\cos(\delta_{ik})) \end{aligned} \tag{2}$$

with

$$G_{ii} := \hat{G}_{ii} + \sum_{k\sim\mathcal{N}_i} G_{ik},\ B_{ii} := \hat{B}_{ii} + \sum_{k\sim\mathcal{N}_i} B_{ik},$$

where $\hat{G}_{ii} \in \mathbb{R}$ and $\hat{B}_{ii} \in \mathbb{R}$ denote the shunt conductance respectively shunt susceptance at node i. The apparent power flow is given by $S_i = P_i + jQ_i$.

3. Modelling of inverters and droop control

We model the inverters as AC voltage sources the amplitude and frequency of which can be defined by the designer [22].[2] We assume that the frequency regulation is instantaneous, but the voltage control happens with a delay that, following standard practice, is represented by a first order filter. Consequently, an inverter at the i–th node is represented by

$$\begin{aligned} \dot{\delta}_i &= u_i^{\delta} \\ \dot{V}_i &= \frac{1}{\tau_{V_i}}(-V_i + u_i^{\mathrm{V}}), \end{aligned} \tag{3}$$

where $u_i^{\delta}, u_i^{V} : \mathbb{R}_{\geq 0} \to \mathbb{R}$ are controls and $\tau_{V_i} \in \mathbb{R}_{>0}$ is the time constant of a low-pass filter.

In contrast to SG units, inverters do not have an inherent physical relation between frequency and generated active power. Frequency droop control aims at artificially creating such a relation, since it is desired in many applications [8]. The rationale behind the droop controller is as follows [3, 11]. For small angular deviations δ_{ik} we have that $\sin(\delta_{ik}) \approx \delta_{ik}$ while $\cos(\delta_{ik}) \approx 1$. Hence, for dominantly inductive networks, *i.e.* $G_{ik} \approx 0$, from the power equations (2) it is clear that the reactive power is more strongly influenced by changes in the voltage, while the active power depends more directly on angular deviations. Consequently, the frequencies ω_i and voltage amplitudes V_i of the inverters are modified depending on the deviations (with respect to a desired value) of the active and reactive powers, respectively.

Simple proportional controller are then implemented as

$$\begin{aligned} u_i^{\delta} &= \omega^d - k_{P_i}(P_i^m - P_i^d) \\ u_i^{V} &= V_i^d - k_{Q_i}(Q_i^m - Q_i^d) \end{aligned} \tag{4}$$

with $\omega^d \in \mathbb{R}_{>0}$ the desired (nominal) frequency, $V_i^d \in \mathbb{R}_{>0}$ the desired (nominal) voltage amplitude, $P_i^m, Q_i^m : \mathbb{R}_{\geq 0} \to \mathbb{R}$ the measured powers, $P_i^d, Q_i^d \in \mathbb{R}$ their desired setpoints and $k_{P_i}, k_{Q_i} \in \mathbb{R}_{>0}$ the frequency and voltage droop gains. It is assumed that the powers are measured and processed through filters [4, 26]

$$\begin{aligned} \tau_{P_i}\dot{P}_i^m &= -P_i^m + P_i \\ \tau_{P_i}\dot{Q}_i^m &= -Q_i^m + Q_i, \end{aligned} \tag{5}$$

where P_i and Q_i are given in (2) and $\tau_{P_i} \in \mathbb{R}_{>0}$ is the time constant of the low pass filters.

Replacing (4) and (5) in (3) yields the closed–loop system

$$\begin{aligned} \dot{\delta}_i &= \omega^d - k_{P_i}(P_i^m - P_i^d) \\ \dot{P}_i^m &= \frac{1}{\tau_{P_i}}(-P_i^m + P_i) \\ \dot{V}_i &= \frac{1}{\tau_{V_i}}(-V_i + V_i^d - k_{Q_i}(Q_i^m - Q_i^d)) \\ \dot{Q}_i^m &= \frac{1}{\tau_{P_i}}(-Q_i^m + Q_i). \end{aligned} \tag{6}$$

[1] To simplify the notation the time argument of all signals is omitted in the sequel.

[2] An underlying assumption to this model is that whenever the inverter connects an intermittent renewable generation source, *e.g.* a photovoltaic plant or a wind plant, to the network, it is equipped with some sort of storage (*e.g.*, flywheel, battery). Thus, it can increase and decrease its power output in a certain range.

In general $\tau_{V_i} \ll \tau_{P_i}$, hence we assume in the sequel $\tau_{V_i} = 0$. Then, the system above reduces to (in analogy to [30])

$$\begin{aligned} \dot{\delta}_i &= \omega_i \\ \tau_{P_i}\dot{\omega}_i &= -\omega_i + \omega^d - k_{P_i}(P_i - P_i^d) \\ \tau_{P_i}\dot{V}_i &= -V_i + V_i^d - k_{Q_i}(Q_i - Q_i^d), \end{aligned} \tag{7}$$

where ω_i denotes the inverter frequency. To simplify the notation we define

$$\begin{aligned} \delta :=& \text{col}(\delta_i) \in \mathbb{S}^n,\ \omega := \text{col}(\omega_i) \in \mathbb{R}^n \\ V :=& \text{col}(V_i) \in \mathbb{R}^n,\ V^d := \text{col}(V_i^d) \in \mathbb{R}^n \\ P^d :=& \text{col}(P_i^d) \in \mathbb{R}^n,\ P := \text{col}(P_i) \in \mathbb{R}^n \\ Q^d :=& \text{col}(Q_i^d) \in \mathbb{R}^n,\ Q := \text{col}(Q_i) \in \mathbb{R}^n \\ T :=& \text{diag}(\tau_{P_i}) \in \mathbb{R}^{n\times n},\ K_P := \text{diag}(k_{P_i}) \in \mathbb{R}^{n\times n} \\ K_Q :=& \text{diag}(k_{Q_i}) \in \mathbb{R}^{n\times n} \end{aligned} \tag{8}$$

and write the system compactly as

$$\begin{aligned} \dot{\delta} &= \omega \\ T\dot{\omega} &= -\omega + \mathbb{1}_n\omega^d - K_P(P - P^d) \\ T\dot{V} &= -V + V^d - K_Q(Q - Q^d) \end{aligned} \tag{9}$$

with power flows P, Q given in (2). We further associate to each inverter its power rating $S_i^N \in \mathbb{R}_{>0}$, $i = 1, \ldots, n$.

Remark 3.1. The desired power setpoints for active and reactive power P_i^d and Q_i^d are assumed to be sent to each inverter $i \in \bar{n}$ by a supervisory control, *i.e.* typically a secondary control or energy management system.

Remark 3.2. Since an inverter may connect a pure storage device, *e.g.*, a battery, to the network, P_i^d can also take negative values. In that case, the storage device is charged depending on the excess power available in the network and thus functions as a frequency and voltage dependent load. In the sequel, we refer to such an operation mode as charging mode.

Remark 3.3. In [30] it is proven that the dynamics of an inverter with frequency droop control and the swing equation dynamics of an SG are equivalent. Consequently, an inverter operated in voltage source mode and with frequency droop achieves a behavior similar to that of an SG with respect to frequency, which is desired in many microgrid applications [19, 8].

Remark 3.4. There are several other alternative droop control schemes proposed in the literature, *e.g.* [36, 12, 11]. The ones proposed here are the most common ones for dominantly inductive networks. We will therefore restrict our analysis to these control laws, commonly denoted by "conventional droop-control".

4. Boundedness of trajectories

The proposition below gives conditions for global boundedness of the trajectories of the system (9), which we recall lives in the set

$$\mathbb{M} := \mathbb{S}^n \times \mathbb{R}^n \times \mathbb{R}^n_{>0}. \tag{10}$$

To establish our result, we need the following assumption on the network susceptances.

Assumption 4.1.

$$B_{ii} \leq \sum_{k\sim\mathcal{N}_i} B_{ik} \text{ for all } i \in \bar{n}. \tag{11}$$

Remark 4.2. Condition (11) holds in general for dominantly inductive networks, on which we focus our analysis.

Proposition 4.3. *Consider the system* (9) *verifying Assumption 4.1. The set* $\mathbb{M}$ *defined in* (10) *is invariant and all trajectories of* (9) *are bounded if* V_i^d, k_{Q_i} *and* Q_i^d *are chosen such that*

$$V_i^d + k_{Q_i}Q_i^d > 0 \tag{12}$$

for all $i \in \bar{n}$.

Proof. From (7), write $\tau_{P_i}\dot{V}_i = f_{3i}(\delta, V)$, for some function $f_{3i} : \mathbb{S}^n \times \mathbb{R}^n_{>0} \to \mathbb{R}$. Note that,

$$f_{3i}(V, \delta)_{|V_i=0} = V_i^d + k_{Q_i}Q_i^d, \tag{13}$$

that, under condition (12), is positive. Hence, the following implication is true

$$V_i(0) > 0 \ \Rightarrow\ V_i(t) > 0, \tag{14}$$

for all $t \geq 0$. This proves that the set $\mathbb{M}$ is invariant.

To establish boundedness of solutions define the matrix $\Gamma := \text{diag}(\tau_{P_i}/k_{Q_i})$, $i \sim \bar{n}$ and the function $W : \mathbb{R}^n \to \mathbb{R}_{>0}$

$$W(V) = \|\Gamma V\|_1 = \sum_{i=1}^n \frac{\tau_{P_i}}{k_{Q_i}} V_i \tag{15}$$

with $\|\cdot\|_1$ the 1–norm. Then,

$$\begin{aligned} \dot{W} &= \sum_{i=1}^n \left(\frac{1}{k_{Q_i}}(-V_i + V_i^d) - (Q_i(\delta, V) - Q_i^d) \right) \\ &\leq -\kappa_1 W + \kappa_2 - V^\top \mathcal{T}(\delta) V, \end{aligned} \tag{16}$$

where

$$\kappa_1 := \min_{i\in\bar{n}} \left\{ \frac{1}{\tau_{P_i}} \right\}, \quad \kappa_2 := \sum_{i=1}^n \left(\frac{1}{k_{Q_i}} V_i^d + Q_i^d \right) \tag{17}$$

and $\mathcal{T} : \mathbb{S}^n \to \mathbb{R}^{n\times n}$ with

$$\begin{aligned} (\mathcal{T}(\delta))_{ii} &:= -B_{ii} \\ (\mathcal{T}(\delta))_{ik} &:= B_{ik}\cos(\delta_{ik}),\ i \neq k. \end{aligned} \tag{18}$$

Here, we have used the fact that equation (2) implies

$$\sum_{i=1}^{n} Q_i = \sum_{i=1}^{n} \left(-B_{ii} V_i^2 + \sum_{k \sim \mathcal{N}_i} B_{ik} V_i V_k \cos(\delta_{ik}) \right), \quad (19)$$

which are the reactive power losses in the network.

Since $B_{ik} = B_{ki}$, $\mathcal{T}(\delta)$ is symmetric and (11) implies that

$$\mathcal{T}(\delta) \geq n \kappa_3 \Gamma^2, \quad (20)$$

for some $\kappa_3 \geq 0$. Hence

$$\dot{W} \leq -\kappa_1 W + \kappa_2 - \kappa_3 W^2, \quad (21)$$

where the third right hand term follows from

$$n V^\top \Gamma^2 V \geq \|\Gamma V\|_1^2 = W^2(V). \quad (22)$$

Assume $\kappa_3 > 0$. The differential equation

$$\dot{z} = -\kappa_1 z + \kappa_2 - \kappa_3 z^2, \quad z(0) = z_0 \quad (23)$$

has solution

$$z(t) = \frac{1}{2\kappa_3} \left[-\kappa_1 + \kappa_4 \tanh(\frac{\kappa_4}{2}(t + \kappa_5)) \right] \quad (24)$$

with $\kappa_4 := \sqrt{4\kappa_2\kappa_3 + \kappa_1^2}$ and

$$\kappa_5 := \frac{2}{\kappa_4} \text{Arctanh} \left(\frac{2\kappa_3 z_0 + \kappa_1}{\kappa_4} \right). \quad (25)$$

From the Comparison Lemma [16] we then have for $W(V(0)) \leq z_0$

$$\sum_{i=1}^{n} \frac{\tau_{P_i}}{k_{Q_i}} V_i(t) \leq -\frac{\kappa_1}{2\kappa_3} + \frac{\kappa_4}{2\kappa_3} \tanh \left[\frac{\kappa_4}{2} (t + \kappa_5) \right], \quad (26)$$

hence $V \in \mathcal{L}_\infty$. This, together with (2), implies that $P \in \mathcal{L}_\infty$. Finally, $\omega \in \mathcal{L}_\infty$ follows from (7), which shows that ω_i is the output of a linear time invariant (LTI) asymptotically stable system with bounded input.

If $\kappa_3 = 0$ we have $\dot{W} \leq -\kappa_1 W + \kappa_2$, and the proof follows immediately.
□□□

Remark 4.4. From (25) and the definition of the Arctanh function it follows that for $z(t)$ in (24) to be well-defined, z_0 and κ_3 must be chosen such that $|2\kappa_3 z_0 + \kappa_1| < \kappa_4$ holds. Recalling that $\kappa_m > 0$ for $m = 1, \ldots, 4$ in (24) simple calculations yield for the initial conditions of interest ($z_0 > 0$)

$$0 < z_0 < \frac{-\kappa_1 + \sqrt{\kappa_1^2 + 4\kappa_2\kappa_3}}{2\kappa_3}. \quad (27)$$

Remark 4.5. Condition (12) in Proposition 4.3 has a clear physical interpretation. Indeed, from the dynamics of V_i in (7) we see that the equilibrium voltage is given by

$$V_i^s = V_i^d - k_{Q_i}(Q_i^s - Q_i^d),$$

where Q_i^s is the reactive power injected in steady state to the i–th bus. Hence, (12) requires that the gains k_{Q_i} and the setpoints V_i^d and Q_i^d of the voltage droop control (4) are chosen such that $V_i^s > 0$ even if there is zero reactive power injection to the i–th bus. Notice that condition (12) is satisfied for all k_{Q_i} if $Q_i^d \geq 0$.

5. Asymptotic stability for lossless microgrids

In this section we derive conditions for asymptotic stability for *lossless microgrids*, *i.e.* $G_{ii} = G_{ik} = 0$ for all $i, k \in \bar{n}$. The assumption of lossless line admittances may be justified as follows: in MV and LV networks the line impedance is usually not purely inductive, but has a non–negligible resistive part. On the other hand, the inverter output impedance is typically inductive (due to the output inductor and/or the possible presence of an output transformer). Under these circumstances, the inductive parts dominate the resistive parts in the admittances for some particular microgrids, especially on the MV level.

We only consider such microgrids and absorb the inverter output admittance (together with the possible transformer admittance), $\tilde{Y}_{ik}$, into the line admittances, Y_{ik}, while neglecting all resistive effects. This assumption is further justified for the present analysis, since the droop control laws introduced in (4) are mostly used in networks with dominantly inductive admittances [12, 11].

For a lossless microgrid with inductive admittances $B_{ik} < 0$ for all $i, k \in \bar{n}$ the power flow equations (2) reduce to

$$\begin{aligned} P_i &= \sum_{k \sim \mathcal{N}_i} |B_{ik}| V_i V_k \sin(\delta_{ik}) \\ Q_i &= |B_{ii}| V_i^2 - \sum_{k \sim \mathcal{N}_i} |B_{ik}| V_i V_k \cos(\delta_{ik}). \end{aligned} \quad (28)$$

Remark 5.1. The need to introduce the, sometimes unrealistic, assumption of lossless admittances has a long history in power systems studies. It appears in transient stability studies, where the presence of transfer conductances hampers the derivation of energy–Lyapunov functions [34]. Although there has been progress in addressing this issue [2, 7], to the best of our knowledge, no analytic solution for power systems with variable frequencies as well as variable voltage amplitudes is available today. See also [23] for an illustration of the deleterious effect of line losses on field excitation controller design.

Remark 5.2. In the case of the Kron–reduced network, we are aware that, in general, the reduced network admittance matrix does not permit to neglect the conductances and our stability results might therefore be inaccurate [34]. Alternatively, one could consider the idealized scenario in which part of the inverter–interfaced storage devices are being charged, hence acting as loads and all constant impedance loads are neglected. Another approach is to use other, possibly dynamic, load models instead of constant impedances in so-called *structure preserving power systems*. However, in the presence of variable voltages the load models are usually, somehow artificially, adapted to fit the theoretical framework used for the construction of energy-Lyapunov functions, see *e.g.* [5, 10].

5.1. Synchronized trajectory

To state the main result of this section we need the following natural power–balance feasibility assumption.

Assumption 5.3. *There exists* $\delta^s \in \Theta$, $\omega^s \in \mathbb{R}$ *and* $V^s \in \mathbb{R}^n_{>0}$, *where*

$$\Theta := \left\{ \delta \in \mathbb{S}^n \;\middle|\; |\delta_{ik}| < \frac{\pi}{2}, i \sim \bar{n},\ k \sim \mathcal{N}_i \right\},$$

such that

$$\begin{aligned} \mathbb{1}_n \omega^s - \mathbb{1}_n \omega^d + K_P[P(\delta^s, V^s) - P^d] &= 0 \\ V^s - V^d + K_Q[Q(\delta^s, V^s) - Q^d] &= 0. \end{aligned} \tag{29}$$

Under Assumption 5.3, the trajectory of the system (9) starting in $(\delta^s, \mathbb{1}_n\omega^s, V^s)$ is given by

$$\begin{aligned} \delta^*(t) &= \mathrm{mod}_{2\pi}\{\delta^s + \mathbb{1}_n \omega^s t\} \\ \omega^*(t) &= \mathbb{1}_n \omega^s \\ V^*(t) &= V^s, \end{aligned} \tag{30}$$

where the operator[3] $\mathrm{mod}_{2\pi}\{\cdot\}$ is added to respect the topology of the system. This desired trajectory is called synchronized trajectory and ω^s is the synchronization frequency.

Remark 5.4. As done in [31] where a similar analysis is made, for lossless networks it is possible to uniquely determine ω^s. Towards this end, recall the well-known fact that in a lossless power system

$$\sum_{i \sim \bar{n}} P_i^s = 0. \tag{31}$$

Thus, replacing the synchronized trajectory in (7) and adding up all the nodes yields

$$\omega^s = \omega^d + \frac{\sum_{i \sim \bar{n}} P_i^d}{\sum_{i \sim \bar{n}} \frac{1}{k_{P_i}}}. \tag{32}$$

Remark 5.5. Clearly, the synchronized trajectory lives in the set $\Theta \times \mathbb{1}_n\omega^s \times \mathbb{R}^n_{>0}$.

5.2. Error dynamics

The main result of this section is to give conditions on the setpoints and gains of the droop controller (4) such that the synchronized trajectory (30) is asymptotically stable. To establish this result we make the important observation that, since the dependence with respect to δ of the dynamics (9) is via angle differences δ_{ik}, the flow is invariant to a shift in the δ coordinate of the form $\delta + \mathbb{1}_n\omega^s t$. Consequently, we can study the stability of the synchronized trajectory (30) in the coordinates

$$\begin{aligned} \tilde{\delta} &= \delta - \mathbb{1}_n \omega^s t \\ \tilde{\omega} &= \omega - \mathbb{1}_n \omega^s, \end{aligned} \tag{33}$$

where—for convenience—we have also shifted the coordinate ω.

Written in the new coordinates the dynamics (9) take the form

$$\begin{aligned} \dot{\tilde{\delta}}_i =& \tilde{\omega}_i \\ \dot{\tilde{\omega}}_i =& \frac{1}{\tau_{P_i}}(-\tilde{\omega}_i - k_{P_i} \sum_{k \sim \mathcal{N}_i} V_i V_k |B_{ik}| \sin(\tilde{\delta}_{ik}) + c_{1_i}) \\ \dot{V}_i =& \frac{1}{\tau_{P_i}}(-V_i - k_{Q_i}|B_{ii}|V_i^2 \\ & + k_{Q_i} \sum_{k \sim \mathcal{N}_i} V_i V_k |B_{ik}| \cos(\tilde{\delta}_{ik}) + c_{2_i}), \end{aligned} \tag{34}$$

where we defined

$$\tilde{\delta}_{ik} := \tilde{\delta}_i - \tilde{\delta}_k,$$

which clearly verifies $\tilde{\delta}_{ik} = \delta_{ik}$, and introduced the constants

$$c_{1_i} := \omega^d - \omega^s + k_{P_i} P_i^d,\ c_{2_i} := V_i^d + k_{Q_i} Q_i^d. \tag{35}$$

Notice that (34) has a (constant) equilibrium at

$$x^s := (\tilde{\delta}^s, \underline{0}_n, V^s), \tag{36}$$

the asymptotic stability of which implies asymptotic stability to the motion associated to the synchronized trajectory.

5.3. Main result

To streamline the presentation of the asymptotic stability result we introduce the constants

$$\kappa_i := \left[\frac{\left(\sum_{k \sim \mathcal{N}_i} V_k^s |B_{ik}| \sin(\tilde{\delta}_{ik}^s) \right)^2}{\sum_{k \sim \mathcal{N}_i} V_k^s |B_{ik}| \cos(\tilde{\delta}_{ik}^s)} - |B_{ii}| V_i^s \right] V_i^s, \tag{37}$$

$i \sim \bar{n}$, where δ^s and V^s are the equilibrium values defined in Assumption 5.3.

Proposition 5.6. *Consider the system* (9) *verifying Assumption 5.3. Fix* k_{P_i} *and* P_i^d. *Select* V_i^d, k_{Q_i} *and* Q_i^d *such that*

$$\frac{V_i^d}{k_{Q_i}} + Q_i^d > \kappa_i. \tag{38}$$

Then, the synchronized motion is asymptotically stable. That is, there exists a neighborhood of x^s, *given in* (36), *such that all trajectories starting in this set are bounded and converge to* x^s.

Proof. The proof is established proving asymptotic stability of the the equilibrium x^s of the "shifted" system representation (34). We follow the interconnection and damping assignment passivity–based control approach [24], and represent the system (34) in port–Hamiltonian form to identify the energy–Lyapunov function.

[3] The operator $\mathrm{mod}_{2\pi}\{\cdot\} : \mathbb{R} \to [0, 2\pi]$, is defined as follows: $y = \mathrm{mod}_{2\pi}\{x\}$ yields $y = x - k2\pi$ for some integer k with $\mathrm{sign}(y) = \mathrm{sign}(x)$ and $y \in [0, 2\pi]$.

Defining $x_i := \text{col}(\tilde{\delta}_i, \tilde{\omega}_i, V_i)$, and $x := \text{col}(x_i)$ we can write (34) as

$$\dot{x} = (J - R(x))\nabla H, \tag{39}$$

where the Hamiltonian $H : \mathbb{R}^n \times \mathbb{R}^n \times \mathbb{R}^n_{>0} \to \mathbb{R}$ is given by

$$\begin{aligned} H(x) = &\sum_{i=1}^{n} \Big(\frac{\tau_{P_i}}{2k_{P_i}} \tilde{\omega}_i^2 - \frac{c_{1_i}}{k_{P_i}} \tilde{\delta}_i + \frac{1}{k_{Q_i}} (V_i - c_{2_i} \ln(V_i)) \\ &+ \frac{1}{2} |B_{ii}| V_i^2 - \frac{1}{2} \sum_{k \sim \mathcal{N}_i} V_i V_k |B_{ik}| \cos(\tilde{\delta}_{ik}) \Big) \end{aligned} \tag{40}$$

and the interconnection and damping matrices are

$$J = \text{blkdiag}(J_i), \quad R(x) = \text{blkdiag}(R_i(x_i)), \quad i \sim \bar{n} \tag{41}$$

with

$$J_i = \begin{bmatrix} 0 & \frac{k_{P_i}}{\tau_{P_i}} & 0 \\ -\frac{k_{P_i}}{\tau_{P_i}} & 0 & 0 \\ 0 & 0 & 0 \end{bmatrix}, R_i = \begin{bmatrix} 0 & 0 & 0 \\ 0 & \frac{k_{P_i}}{\tau_{P_i}^2} & 0 \\ 0 & 0 & \frac{k_{Q_i} V_i}{\tau_{P_i}} \end{bmatrix}. \tag{42}$$

Notice that $J = -J^\top$ and $R \geq 0$. Consequently,

$$\dot{H} = -(\nabla H)^\top R \nabla H \leq 0. \tag{43}$$

Therefore, x^s is a stable equilibrium of system (39) if $H(x)$ has a strict local minimum at the equilibrium x^s. To ensure the latter we show that $\nabla H(x^s) = \underline{0}_{3n}$ and $\frac{\partial^2 H(x)}{\partial x^2}\big|_{x^s} > 0$. Now,

$$\frac{\partial H(x)}{\partial x_i}\Big|_{x^s} = \begin{bmatrix} V_i^s a_i - \frac{c_{1_i}}{k_{P_i}} \\ 0 \\ -b_i + |B_{ii}| V_i^s + \frac{1}{k_{Q_i}} \left(1 - \frac{c_{2_i}}{V_i^s}\right) \end{bmatrix}^\top, \tag{44}$$

where we defined

$$\begin{aligned} a_i &:= \sum_{k \sim \mathcal{N}_i} V_k^s |B_{ik}| \sin(\tilde{\delta}_{ik}^s) \\ b_i &:= \sum_{k \sim \mathcal{N}_i} V_k^s |B_{ik}| \cos(\tilde{\delta}_{ik}^s). \end{aligned}$$

Hence, $\nabla H(x^s) = \underline{0}_{3n}$.

Showing that $\frac{\partial^2 H(x)}{\partial x^2}\big|_{x^s} > 0$ is equivalent to showing that $\frac{\partial^2 H(x)}{\partial x_i^2}\big|_{x^s} > 0$ for all $i \in \bar{n}$. Some simple computations yield

$$\frac{\partial^2 H(x)}{\partial x_i^2}\Big|_{x^s} = \begin{bmatrix} V_i^s b_i & 0 & a_i \\ 0 & \frac{\tau_{P_i}}{k_{P_i}} & 0 \\ a_i & 0 & |B_{ii}| + \frac{c_{2_i}}{k_{Q_i}(V_i^s)^2} \end{bmatrix}. \tag{45}$$

Clearly, this matrix is positive definite if the submatrix

$$\begin{bmatrix} V_i^s b_i & a_i \\ a_i & |B_{ii}| + \frac{c_{2_i}}{k_{Q_i}(V_i^s)^2} \end{bmatrix} \tag{46}$$

is positive definite. Now, since $\tilde{\delta}^s \in \Theta$ we have that $b_i > 0$. Finally, it can be shown that the determinant is positive if and only if

$$|B_{ii}| V_i^s + \frac{c_{2_i}}{k_{Q_i} V_i^s} > \frac{a_i^2}{b_i}, \tag{47}$$

which by recalling $\tilde{\delta}_{ik}^s = \delta_{ik}^s$ and the definition of c_{2_i} in (35), leads to the condition (38).

Recalling (43) and the fact that $R(x) \geq 0$, we see that to prove asymptotic stability it suffices to show that—along the trajectories of the system —the implication below holds

$$R(x(t))\nabla H(x(t)) \equiv \underline{0}_{3n} \Rightarrow \lim_{t \to \infty} x(t) = x^s. \tag{48}$$

From (48) it follows that

$$\frac{\partial H}{\partial x_{i_2}} = 0, \ \frac{\partial H}{\partial x_{i_3}} = 0, \tag{49}$$

where the first condition implies $x_{i_2} = 0$. Hence, x_{i_1} is constant. The second condition implies x_{i_3} is constant. Therefore, the invariant set where $\dot{H}(x(t)) \equiv 0$ is an equilibrium. To prove that this is the desired equilibrium x^s we recall that x^s is an isolated minimum of $H(x)$. Consequently, there is a neighborhood of x^s where no other equilibrium exists, completing the proof.

□□□

Remark 5.7. Our analysis reveals that local stability of the lossless microgrid (9) is independent of the frequency droop gains k_{P_i}, active power setpoints P_i^d and low pass filter time constants τ_{P_i}, and only condition (38) is imposed on V_i^d, k_{Q_i} and Q_i^d. In that regard, the result is identical to those derived for lossless first–order inverter models in [31] and lossless second–order inverter models in [30], both assuming constant voltage amplitudes.

Remark 5.8. Condition (38) is imposed to ensure $H(x)$ is a positive definite function and, therefore, qualifies as a Lyapunov function candidate. This condition can be removed if, instead of Lyapunov theory, La Salle's invariance principle (that does not require positive definiteness) is invoked [16]. Indeed, from the proof of Proposition 5.6 we have that the function $H(x)$ is still non–increasing and via La Salle we can conclude that all *bounded* trajectories converge to an equilibrium. Unfortunately, this property is of little interest at this point because, even though in Proposition 4.3 we prove global boundedness of the state (δ, ω, V), there is no obvious way to conclude that the state x—that consists of incremental variables—is bounded.

6. Active power sharing

In [31] a criterion on the frequency droop gains and setpoints has been derived such that the generation units share the active power according to their power ratings.

This is a desired control goal in many applications. However, it has been argued in [6] that system operators may not always seek to achieve a power sharing in proportion to the power ratings of the units. Instead they may also wish to take into account other technical, economic or environmental criteria, such as fuel consumption, generation costs or emission costs, see also [15].

In this regard, the ideas derived in [31] are easily applied to proportional active power sharing with respect to a user-defined criterion. It turns out that the same criterion ensures that storage devices in charging mode, *i.e.* $P_i^d < 0$ for some $i \in \bar{n}$, are charged proportionally. To formulate the selection criterion for the controller gains and setpoints, we employ the following definition.

Definition 6.1. *Let χ_i, $i = 1, \ldots, n$ denote the active power sharing performance criterion. Then, two inverters at nodes $i, k \in \bar{n}$ share their active powers proportionally if*

$$\frac{P_i^s}{\chi_i} = \frac{P_k^s}{\chi_k}. \tag{50}$$

Remark 6.2. One possible power sharing performance criterion would, *e.g.*, be $\chi_i = S_i^N$, $i = 1, \ldots, n$. However, the power sharing performance criterion χ_i do not have to be equal for all inverters in general. Thus, active power could, *e.g.*, be shared according to an economic or environmental criteria by some inverters, while it could be shared according to the power ratings by other inverters.

Lemma 6.3. *Consider the system* (9) *verifying Assumption 5.3. Then, all inverters the power outputs of which satisfy sign(P_i^s) = sign(P_k^s), share the active power proportionally if the gains k_{P_i}, k_{P_k} and active power setpoints P_i^d, P_k^d are chosen such that*

$$k_{P_i}/\chi_i = k_{P_k}/\chi_k \text{ and } P_i^d/\chi_i = P_k^d/\chi_k \tag{51}$$

for all $i, k \in \bar{n}$ with sign(P_i^s) = sign(P_k^s).

Proof. The claim follows in a straighforward manner from [31], where it has been shown for first-order inverter models and $\chi_i = S_i^N$, $P_i^d > 0$, $P_i^s > 0$, $i = 1, \ldots, n$. Under conditions (51), we have along the synchronized trajectory defined in Assumption 5.3,

$$\frac{P_i^s}{\chi_i} = \frac{P_i^d - k_{P_i}^{-1}(\omega^s - \omega^d)}{\chi_i} = \frac{P_k^d - k_{P_k}^{-1}(\omega^s - \omega^d)}{\chi_k} = \frac{P_k^s}{\chi_k}, \tag{52}$$

where $i, k \in \bar{n}$. □□□

Remark 6.4. For $\chi_i = S_i^N$ conditions (51) imply that the inverters share the power demand in proportion to their power ratings if their droop gains and power setpoints are chosen equally in inverter per unit values.

Remark 6.5. The conditions in Lemma 6.3 also imply that storage devices in charging mode are charged proportionally.

Remark 6.6. Note that proportional active power sharing is achieved by Lemma 6.3 independently of the admittance values of the network. However, in a highly ohmic network, the droop control laws (4) may induce high fluctuating currents due to the stronger coupling of phase angles and reactive power, see (2). Then, additional methods such as the virtual output impedance [13] or alternative droop control laws [36] could be employed instead of (4).

Remark 6.7. As described in Section 3, the voltage droop control law (4) follows a similar heuristic approach as the frequency control droop law, aiming at obtaining a desired reactive power distribution in a synchronized state. However, the conditions for proportional power sharing in Lemma 6.3 are derived using the fact that the frequency is equal all over the network for a synchronized trajectory, *i.e.* $\omega_i^s = \omega_k^s = \ldots = \omega^s$, and serves thus as a common communication signal. This is not the case for the voltage droop, since in general $V_i^s \neq V_k^s$ for $i, k \in \bar{n}$. In the special case of equal voltage amplitudes, *i.e.* $V_i^s = V_k^s$, $i, k \in \bar{n}$, proportional reactive power sharing can be achieved by selecting $V_i^d = V_k^d$ as well as reactive droop gains k_{Q_i}, k_{Q_k} and setpoints Q_i^d, Q_k^d following Lemma 6.3. The fact that the voltage droop control (4) does not in general achieve proportional reactive power sharing has been widely recognized in the literature and several alternative or modified decentralized droop control structures have been proposed, *e.g.* in [21, 35], with the purpose of improving the reactive power sharing. Nevertheless, proportional reactive power sharing via a decentralized control law is still a challenging open question.

7. Simulation example

Our theoretical analysis is illustrated next via a simulation example based on the three-phase islanded Subnetwork 1 of the CIGRE benchmark medium voltage distribution network [27]. The network is a meshed network and consists of 11 main buses, see Fig. 1.

The following two modifications are made compared to the original system given in [27]: first, at bus 9b the combined head and power (CHP) diesel generator is replaced by an inverter-interfaced CHP fuel cell (FC). Second, since the original network given in [27] stems from a distribution network connected to a transmission system, the power ratings of the generation units are scaled by a factor 4 compared to [27], such that the controllable units (CHPs, batteries, FC) can satisfy the load demand in autonomous operation mode at least during some period of time.

The network in Fig. 1 possesses a total of six controllable generation sources of which two are batteries at buses 5b ($i = 1$), respectively 10b ($i = 5$), two are FCs in households at buses 5c ($i = 2$), respectively 10c ($i = 6$) and two are FC CHPs at buses 9b ($i = 5$) and 9c ($i = 4$). We assume that all controllable generation units are equipped with frequency and voltage droop control as

given in (4). We associate to each inverter its power rating S_i^N, $i \in \bar{n}$. Since the apparent power ratings of the generation sources are not specified in [27], we set S_i^N to the maximum active power given for each source in [27], Table 2. The transformer impedances of the inverter-interfaced units are modelled with $R_{T_i} = 0.01 S_{\text{base}}/S_i^N$ pu, $X_{T_i} = 0.06 S_{\text{base}}/S_i^N$ pu, $i \in \bar{n}$, where pu denotes per unit values with respect to the common system base power S_{base} given in Table 1. Here, we assumed for simplicity that the transformer power rating is equivalent to the power rating of the corresponding inverter S_i^N, $i \in \bar{n}$. The output filter inductances are assumed equal to $X_F = 0.0005$ pu for all units.

Non-controllable PV units are connected at buses 3, 4, 6, 8 and 11. The loads at nodes 3-11 represent industrial and household loads as specified in [27], Table 1, besides the load at node 1, which is neglected. The line parameters and lengths are as given in [27], Table 3. The total lengths of the lines is approximately 15 km. We consider the following two scenarios.

1) Lossless scenario. All loads and uncontrollable generation sources (PV, wind turbine) of the test system given in Fig. 1 are neglected. As outlined in Section 5, we merge the transfomer and filter impedances of the inverters with the line impedances. The largest R/X ratio of an admittance in the network is then 0.21. For HV transmission lines it is typically 0.31 [8]. Hence, the assumption of dominantly inductive admittances is satisfied. Consequently, the droop control laws given in (4) are adequate and our stability analysis of Section 5 applies.

The batteries at nodes 5b and 10b are operated in charging mode, hence functioning as loads. We design the active power droop gains and setpoints of the inverters according to Lemma 6.3 with $\chi_i = S_i^N$, $P_i^d = \alpha_i S_{b_i}/S_{\text{base}}$ pu, $k_{P_i} = 0.1 S_{\text{base}}/S_{b_i}$ Hz/pu for all $i \in \bar{n}$, i.e. the inverters should supply the requested power, respectively be charged, in proportion to their power ratings. We assume the power setpoints have been provided by some sort of supervisory control or energy management system, see Remark 3.1, with $\alpha_i = 0.7$ for inverters in generation mode ($i = 2, 3, 4, 6$) and $\alpha_i = -0.5$ for inverters in charging mode, i.e. $i = 1, 5$.

The reactive power setpoints are set to $Q_i^d = \beta_i S_{b_i}/S_{\text{base}}$ pu with $\beta_i = 0.01$ for all $i \in \bar{n}$ to account for the inductive behavior of the lines. The reactive power droop gains are chosen in the same relation as the active power droop gains, i.e. $k_{Q_i} = 0.2 S_{\text{base}}/S_{b_i}$ pu/pu and $V_i^d = 1$ pu for all $i \in \bar{n}$. The low pass filter time constants are set to $\tau_{P_i} = 0.5$ s, $i \sim \bar{n}$. The main system data and control gains are given in Table 1.

The simulation results are shown in Fig. 2. After a transient the frequencies synchronize and the voltage amplitudes become constant. The latter satisfy the usual requirement of $0.9 < V_i^s < 1.1$ for V_i^s in pu, $i \sim \bar{n}$. The initial conditions have been chosen arbitrarily. Since condition (38) holds for all inverters, the synchronized trajectory is locally asymptotically stable.

The deviation of the synchronization frequency with respect to the nominal frequency is $\omega^s - \omega^d = -4.42$ mHz. Following Remark 5.4, for a purely lossless network with the parameters given in Table 1, the frequency deviation should be $\omega^s - \omega^d = -0.09$ mHz. The higher frequency deviation in the simulation is due to the losses over the lines given by $\sum_{i \sim \bar{n}} P_i^s = 0.05$ pu, from which it follows (in analogy to Remark 5.4) that

$$\omega^s - \omega^d = \frac{\sum_{i \sim \bar{n}} \left(P_i^d - P_i^s\right)}{\sum_{i \sim \bar{n}} \frac{1}{k_{P_i}}} = -4.42 \text{ mHz}. \tag{53}$$

The batteries are charged in proportion to their power ratings with the active power also being supplied proportionally, as stated in Lemma 6.3. Hence, the simulation confirms that the active power droop control, as given in (4), is suited to achieve the desired objective of active power sharing. Regarding the reactive power sharing, we make the following observation. The voltage amplitudes of inverter-interfaced units at the same main buses $5, 9, 10$ become (almost) equal when the system synchronizes. But, as discussed in Section 6, the reactive power is not shared proportionally, limiting the overall performance of the voltage-reactive power droop law (4).

Our experience in numerous simulations with large variety of control gains, setpoints, low pass filter time constants and initial conditions is that whenever the system reaches a synchronized trajectory as defined in Assumption 5.3, the latter is locally asymptotically stable by condition (38). However, there exist gain settings such that the system converges to a limit-cycle behavior. As one would expect, this is the case for large control gains and low pass filter time constants.

2) Scenario with constant impedance loads. In this simulation scenario we evaluate the robustness of our stability condition with respect to loads represented by constant impedances. We therefore assume all PV units work at 50% of their nominal power with $\cos(\phi) := P/S = 0.98$ and are treated as negative loads, while the wind turbine is not generating any power. All loads are represented by constant impedances to ground, the values of which are calculated at nominal frequency and voltage.

At first, we compute the admittance matrix of the equivalent Kron-reduced network. In the present case the largest R/X ratio is 0.22. Thus, the assumption of dominantly inductive admittances is satisfied – even in the presence of impedances representing loads – but of course the term lossless system is no longer adequate. The control gains are chosen as specified in the lossless scenario with $\alpha_i = 0.65$ and $\beta_i = 0.25$, $i = 1, \ldots, 6$. Hence, all inverters operate in generation mode. The voltage setpoints and low pass filter time constants are as in the lossless case. We again assume the power setpoints have been provided by some sort of supervisory control or energy management system. The main data is given in Table 2.

The simulation results are displayed in Fig. 3. All trajectories converge to a synchronized trajectory satisfying

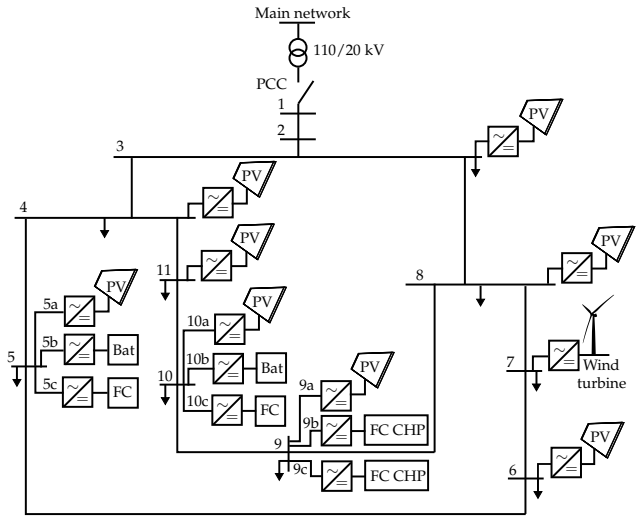

Figure 1: 20 kV MV benchmark model adapted from [27] with 11 main buses and inverter-interfaced units of type: PV-Photovoltaic, FC-fuel cell, Bat-battery, CHP fuel cell. PCC denotes the point of common coupling to the main grid. The sign ↓ denotes loads. The numbering of the main buses is according to [27].

Table 1: Test system parameters for lossless scenario, $i = 1, \ldots, 6$.

Base values	$S_{\text{base}} = 4.75$ MVA, $V_{\text{base}} = 20$ kV
S_i^N	$[0.505, 0.028, 0.261, 0.179, 0.168, 0.012]$ pu
P_i^d	$[-0.253, 0.020, 0.183, 0.125, -0.084, 0.008]$ pu
k_{P_i}	$[0.198, 3.599, 0.383, 0.560, 0.594, 8.482]$ $\frac{\text{Hz}}{\text{pu}}$
Q_i^d	$[0.005, 0.000, 0.003, 0.002, 0.002, 0.000]$ pu
k_{Q_i}	$[0.396, 7.197, 0.766, 1.120, 1.188, 16.964]$ $\frac{\text{pu}}{\text{pu}}$

Table 2: Test system parameters for lossy scenario with loads represented by constant impedances, $i = 1, \ldots, 6$.

Base values	$S_{\text{base}} = 4.75$ MVA, $V_{\text{base}} = 20$ kV
Max. sys. load	0.91+j0.30 pu
Total PV gen.	0.15 pu
S_i^N	$[0.505, 0.028, 0.261, 0.179, 0.168, 0.012]$ pu
P_i^d	$[0.328, 0.018, 0.170, 0.116, 0.110, 0.008]$ pu
k_{P_i}	$[0.198, 3.599, 0.383, 0.560, 0.594, 8.482]$ $\frac{\text{Hz}}{\text{pu}}$
Q_i^d	$[0.126, 0.007, 0.065, 0.045, 0.042, 0.003]$ pu
k_{Q_i}	$[0.396, 7.197, 0.766, 1.120, 1.188, 16.964]$ $\frac{\text{pu}}{\text{pu}}$

condition (38), indicating that the condition is robust – to a certain extent – to the presence of transfer and load conductances. The inverters share the active power demand of the loads as stated in Lemma 6.3. Compared to the lossless scenario, all inverters provide positive reactive power and the voltage amplitudes are equal at all units connected to the same main buses $(5, 9, 10)$, when the system synchronizes. Hence, since the control gains and setpoints have been selected according to Lemma 6.3, generation units connected in parallel to the same main bus $(5, 9, 10)$ share the reactive power in proportion to their ratings (see Remark 6.7). However, as in the lossless scenario, the reactive power sharing is not proportional with respect to all units, since the voltage amplitudes are not equal at all buses.

We have found this behavior of the voltage amplitudes for all tested initial conditions and control parameters satisfying Lemma 6.3 in the presence of inductive loads. We wish to point out, however, that (at the moment) we do not have conditions under which equal voltage amplitudes at generators in parallel (and therefore proportional reactive power sharing) can be achieved via the droop control law (4).

Furthermore, numerous simulations with different parameters indicate that our stability condition (38) is satisfied in all cases in which the system reaches a synchronized trajectory. As in the lossless case, there are gain settings such that the system does not reach a desired synchronized trajectory as defined in Assumption 5.3, but shows a limit cycle behavior. This is typically the case for large control gains and/or large low pass filter time constants.

All simulations are carried out in Plecs [25].

8. Conclusions and future work

We have considered the problem of frequency and voltage stability in a droop-controlled inverter-based microgrid. First, we have shown that the trajectories of the system are globally bounded for all practical choices of controller gains and setpoints. We then have derived sufficient local asymptotic stability conditions for a lossless microgrid via a port-Hamiltonian representation of the latter. Our condition states that local stability is independent of the choice of the controller gains and setpoints of the frequency droop controller as well as low pass filter time constants, but does depend on the choice of the controller gains and setpoints of the voltage droop controller. We further give a design criterion on the controller gains such that a desired active power distribution is achieved in steady-state.

To illustrate our theoretical analysis we provide a simulation example based on the the CIGRE benchmark MV distribution network. The derived stability condition is satisfied and a desired steady-state active power distribution is achieved in simulation for a wide selection of different control gains, setpoints, low pass filter time constants and initial conditions.

Our simulations also show that, despite the observation that meshed microgrids with droop-control possess a locally stable synchronized trajectory for a wide range of control gains, the conventional reactive power droop control does not guarantee proportional reactive power sharing in general. Therefore, future work concerns – possibly distributed – control solutions for accurate reactive power sharing, while guaranteeing network stability. Furthermore, power sharing and stability in dominantly ohmic microgrids is an interesting outstanding problem.

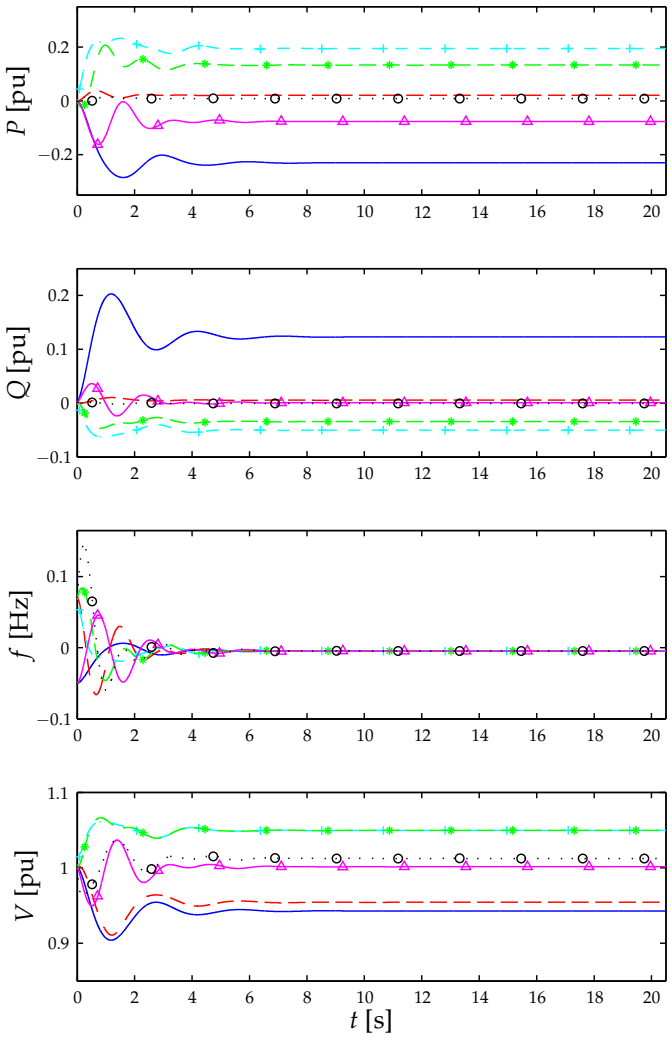

Figure 2: Lossless scenario. Trajectories of the power outputs P_i, Q_i in pu, internal relative frequencies $f_i = (\omega_i - \omega^d)/(2\pi)$ in Hz and voltage amplitudes V_i in RMS of the controllable sources in the microgrid given in Fig. 1, $i = 1, \ldots, 6$. The batteries at nodes 5b respectively 10b operate in charging mode, hence functioning as frequency and voltage dependent loads. The lines correspond to the following sources: Battery 5b, $i = 1$ '–', FC 5c, $i = 2$ '- -', FC CHP 9b, $i = 3$ '+-', FC CHP 9c, $i = 4$ '* -', battery 10b, $i = 5$ '△ -' and FC 10c, $i = 6$ 'o-'. The initial conditions have been chosen arbitrarily. All trajectories converge to a locally aymptotically stable synchronized trajectory satisfying condition (38). The voltage amplitudes remain within 1 ± 0.1 pu in steady-state.

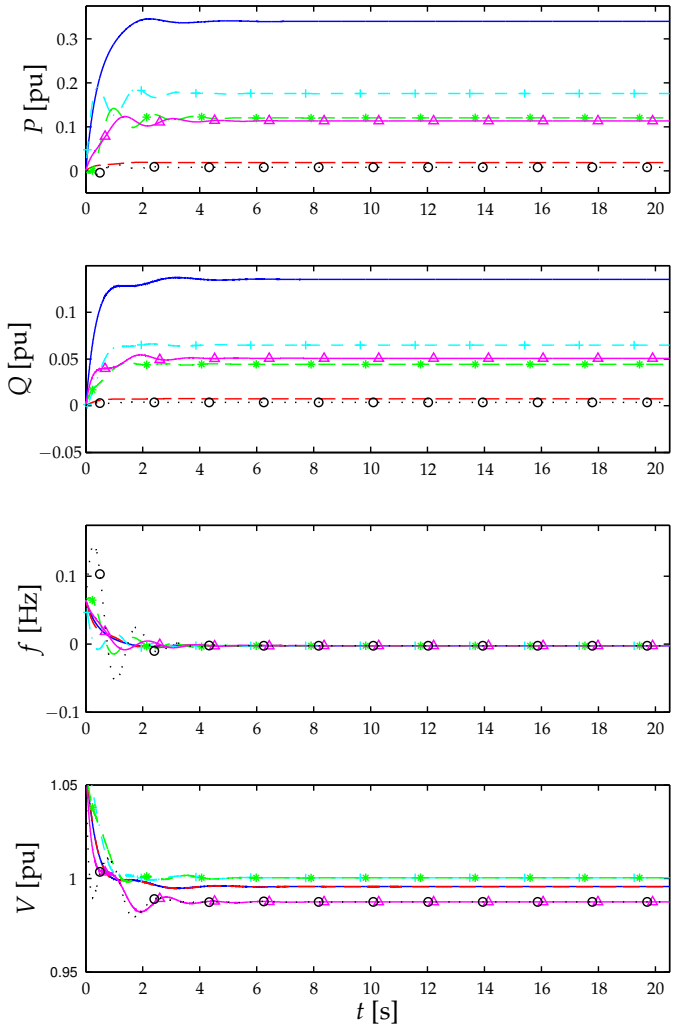

Figure 3: Scenario with constant impedance loads. Trajectories of the power outputs P_i, Q_i in pu, internal relative frequencies $f_i = (\omega_i - \omega^d)/(2\pi)$ in Hz and voltage amplitudes V_i in RMS of the controllable sources in the microgrid given in Fig. 1, $i = 1, \ldots, 6$. The lines correspond to the following sources: Battery 5b, $i = 1$ '–', FC 5c, $i = 2$ '- -', FC CHP 9b, $i = 3$ '+-', FC CHP 9c, $i = 4$ '* -', battery 10b, $i = 5$ '△ -' and FC 10c, $i = 6$ 'o-'. The initial conditions have been chosen arbitrarily. All trajectories converge to a synchronized trajectory satisfying condition (38) indicating that the condition is robust – to a certain extent – to the presence of transfer and load conductances. The voltage amplitudes of units connected to the same main buses ($i = 5, 9, 10$) become equal, when the system synchronizes and at those buses the reactive power sharing is also proportional.

References

[1] Barklund, E., Pogaku, N., Prodanovic, M., Hernandez-Aramburo, C., & Green, T. (2008). Energy management in autonomous microgrid using stability-constrained droop control of inverters. *IEEE Trans. on Power Electronics*, *23*, 2346 –2352.

[2] Bretas, N., & Alberto, L. F. C. (2003). Lyapunov function for power systems with transfer conductances: extension of the invariance principle. *IEEE Trans. on Power Systems*, *18*, 769–777.

[3] Chandorkar, M., Divan, D., & Adapa, R. (1993). Control of parallel connected inverters in standalone AC supply systems. *IEEE Trans. on Industry Applications*, *29*, 136 –143.

[4] Coelho, E., Cortizo, P., & Garcia, P. (2002). Small-signal stability for parallel-connected inverters in stand-alone AC supply systems. *IEEE Trans. on Industry Applications*, *38*, 533 –542.

[5] Davy, R. J., & Hiskens, I. A. (1997). Lyapunov functions for multimachine power systems with dynamic loads. *IEEE Trans. on Circuits and Systems I: Fundamental Theory and Applications*, *44*, 796–812.

[6] Diaz, G., Gonzalez-Moran, C., Gomez-Aleixandre, J., & Diez, A. (2010). Scheduling of droop coefficients for frequency and voltage regulation in isolated microgrids. *IEEE Trans. on Power Systems*, *25*, 489 –496.

[7] Dörfler, F., & Bullo, F. (2012). Synchronization and transient stability in power networks and non-uniform Kuramoto oscillators. *SIAM Journal on Control and Optimization*, *50*, 1616–

1642.

[8] Engler, A. (2005). Applicability of droops in low voltage grids. *International Journal of Distributed Energy Resources*, *1*, 1–6.

[9] Farhangi, H. (2010). The path of the smart grid. *IEEE Power and Energy Magazine*, *8*, 18 –28.

[10] Guedes, R., Silva, F., Alberto, L., & Bretas, N. (2005). Large disturbance voltage stability assessment using extended lyapunov function and considering voltage dependent active loads. In *IEEE PESGM* (pp. 1760–1767).

[11] Guerrero, J., Loh, P., Chandorkar, M., & Lee, T. (2013). Advanced control architectures for intelligent microgrids – part I: Decentralized and hierarchical control. *IEEE Trans. on Industrial Electronics*, *60*, 1254–1262.

[12] Guerrero, J., Matas, J., de Vicuna, L. G., Castilla, M., & Miret, J. (2007). Decentralized control for parallel operation of distributed generation inverters using resistive output impedance. *IEEE Trans. on Industrial Electronics*, *54*, 994 –1004.

[13] Guerrero, J., Garcia de Vicuna, L., Matas, J., Castilla, M., & Miret, J. (2005). Output impedance design of parallel-connected UPS inverters with wireless load-sharing control. *IEEE Trans. on Industrial Electronics*, *52*, 1126 – 1135.

[14] Hatziargyriou, N., Asano, H., Iravani, R., & Marnay, C. (2007). Microgrids. *IEEE Power and Energy Magazine*, *5*, 78 –94.

[15] Hernandez-Aramburo, C., Green, T., & Mugniot, N. (2005). Fuel consumption minimization of a microgrid. *IEEE Trans. on Industry Applications*, *41*, 673 – 681.

[16] Khalil, H. K. (2002). *Nonlinear systems* volume 3. Prentice Hall.

[17] Kundur, P. (1994). *Power system stability and control*. McGraw-Hill.

[18] Kundur, P., Paserba, J., Ajjarapu, V., Andersson, G., Bose, A., Canizares, C., Hatziargyriou, N., Hill, D., Stankovic, A., Taylor, C., Van Cutsem, T., & Vittal, V. (2004). Definition and classification of power system stability IEEE/CIGRE joint task force on stability terms and definitions. *IEEE Trans. on Power Systems*, *19*, 1387–1401.

[19] Lasseter, R. (2002). Microgrids. In *IEEE Power Engineering Society Winter Meeting, 2002* (pp. 305 – 308 vol.1). volume 1.

[20] Lasseter, R. H. (2011). Smart distribution: Coupled microgrids. *Proceedings of the IEEE*, *99*, 1074–1082.

[21] Li, Y. W., & Kao, C.-N. (2009). An accurate power control strategy for power-electronics-interfaced distributed generation units operating in a low-voltage multibus microgrid. *IEEE Trans. on Power Electronics*, *24*, 2977 –2988.

[22] Lopes, J., Moreira, C., & Madureira, A. (2006). Defining control strategies for microgrids islanded operation. *IEEE Trans. on Power Systems*, *21*, 916 – 924.

[23] Ortega, R., Galaz, M., Astolfi, A., Sun, Y., & Shen, T. (2005). Transient stabilization of multimachine power systems with nontrivial transfer conductances. *IEEE Trans. on Automatic Control*, *50*, 60 – 75.

[24] Ortega, R., van der Schaft, A., Maschke, B., & Escobar, G. (2002). Interconnection and damping assignment passivity-based control of port-controlled Hamiltonian systems. *Automatica*, *38*, 585–596.

[25] Plexim GmbH (2013). Plecs software, www.plexim.com.

[26] Pogaku, N., Prodanovic, M., & Green, T. (2007). Modeling, analysis and testing of autonomous operation of an inverter-based microgrid. *IEEE Trans. on Power Electronics*, *22*, 613 –625.

[27] Rudion, K., Orths, A., Styczynski, Z., & Strunz, K. (2006). Design of benchmark of medium voltage distribution network for investigation of DG integration. In *IEEE PESGM* (p. 6 pp.).

[28] van der Schaft, A. (2000). *L2-Gain and Passivity Techniques in Nonlinear Control*. Springer.

[29] Schiffer, J., Anta, A., Trung, T. D., Raisch, J., & Sezi, T. (2012). On power sharing and stability in autonomous inverter-based microgrids. In *Proc. 51st IEEE CDC*. Maui, HI, USA.

[30] Schiffer, J., Goldin, D., Raisch, J., & Sezi, T. (2013). Synchronization of droop-controlled autonomous microgrids with distributed rotational and electronic generation. Submitted to 52nd IEEE CDC, Florence, Italy.

[31] Simpson-Porco, J. W., Dörfler, F., & Bullo, F. (2012). Synchronization and power sharing for droop-controlled inverters in islanded microgrids. *Automatica*, *Accepted*.

[32] Simpson-Porco, J. W., Dörfler, F., & Bullo, F. (2013). Voltage stabilization in microgrids using quadratic droop control. Submitted to 52nd IEEE CDC, Florence, Italy.

[33] Soultanis, N. L., Papathanasiou, S. A., & Hatziargyriou, N. D. (2007). A stability algorithm for the dynamic analysis of inverter dominated unbalanced LV microgrids. *IEEE Trans. on Power Systems*, *22*, 294 –304.

[34] Varaiya, P., Wu, F. F., & Chen, R.-L. (1985). Direct methods for transient stability analysis of power systems: Recent results. *Proceedings of the IEEE*, *73*, 1703–1715.

[35] Yao, W., Chen, M., Matas, J., Guerrero, J., & Qian, Z.-M. (2011). Design and analysis of the droop control method for parallel inverters considering the impact of the complex impedance on the power sharing. *IEEE Trans. on Industrial Electronics*, *58*, 576 –588.

[36] Zhong, Q.-C. (2013). Robust droop controller for accurate proportional load sharing among inverters operated in parallel. *IEEE Trans. on Industrial Electronics*, *60*, 1281–1290.